

PAPER • OPEN ACCESS

Performance analysis of solar updraft tower using Ansys fluent

To cite this article: G Anilkumar *et al* 2020 *IOP Conf. Ser.: Mater. Sci. Eng.* **937** 012022

View the [article online](#) for updates and enhancements.



ECS **240th ECS Meeting**
Oct 10-14, 2021, Orlando, Florida

**Register early and save
up to 20% on registration costs**

Early registration deadline Sep 13

REGISTER NOW

Performance analysis of solar updraft tower using Ansys fluent

G Anilkumar^{1*}, G R Krishna², G V Brahmendra Kumar³ and K Palanisamy⁴

^{1,2} School of Renewable Energy, JNT University, Kakinada, 533003, India

^{3,4} Centre for Smart Grid Technologies, Vellore Institute of Technology, Vellore, 632014, India.

Email: brahmendrakumar.g@gmail.com, kpalanisamy@vit.ac.in

*Corresponding author: gorantlaanilkumar@gmail.com

Abstract. The solar updraft tower (SUT) is a renewable energy power plant design concept for generating electricity by utilizing convective air flow due to low temperature heat absorption from incoming solar radiation. A parametric study on the performance power output of the SUT at various canopy angles and different insolation levels were carried out to investigate the relationship between them with respect to key parameters i.e. in terms of updraft tower velocity, temperature, pressure and height to choose turbine position for maximum air velocity absorption and energy conversion using Ansys-fluent software version 15 for analysis. The results obtained were analyzed comparatively to draw conclusions. The results identified using simulation software mentioned above were validated with earlier results and identified significant improvement in the power generated at various collector angles, when compared with the earlier works on SUT.

1. Introduction

Allocation Solar Updraft Tower (SUT) utilizes three basic governing principles i.e. greenhouse effect, convection and wind power generation to convert incoming solar radiation into electricity [1]. As direct and diffuse solar radiation strikes the surface of glass roof or canopy, reflection, refraction, transmission and absorption take place depending on the incidence angle and optical characteristics of the canopy which can be measured in terms of physical parameters like refractive index, thickness and extinction coefficient [2]. Apart of the transmitted radiation through canopy was absorbed while another part gets reflected back towards the canopy and undergoes further reflection[3-6]. This leads to multiple reflections in-between canopy and surface of the ground so that enhanced energy absorption takes place at the surface of the ground due to transmittance-absorptance product of the ground resulting in production of hot air beneath the canopy. The buoyant air rises up in plant chimney by natural convection and initiates forced convection by allowing more amount of air to flow with in the vicinity of canopy [7-12]. Through mixed convection, the lower part of canopy gets heated up due to presence of warm air while a part of energy is absorbed by the cooler part of the ground surface in addition to radiation exchange between warm ground surface and canopy [13-20]. Further, due to natural and forced convection, heat exchange occurs



over canopy surface with adjacent ambient air. While the air parcels flow upward from canopy to chimney, its temperature increases and velocity remains constant due to increase in height of the canopy [21,22]. Finally, air parcels get cooled at the terminal walls of the chimney where heat energy is converted into kinetic energy [23-30]. The difference in pressure across the chimney base and its outlet can be known by measuring density difference of respective air parcels which in turn depend on associated inlet and outlet temperatures across the chimney. The requisite pressure difference required to drive the turbine can be regulated by minimizing chimney's entrance, exit and friction losses. As the air passes through the turbine, the kinetic energy associated with it drives the turbine blades which in turn drive the generator [30-35].

2. Methodology

The objective of this work is to develop a simplified design model of solar updraft tower power plant to investigate the effects of the canopy angle engulfment and turbine location on fluid flow. Decreasing the overall tower height would decrease the overall construction cost and improve the appearance of the chimney which leads to decreased power output and reduced efficiency of the system. This indicates that there is a scope for optimization. Thus, in search of optimizing the same, the goal of this work is to conduct parametric study and identify maximum power output by varying canopy orientation with respect to ground at various insolation levels using simplified two-dimensional simulation model based on Ansys fluent version 15 software [2].

3. Solar updraft tower design

The experimental prototype of SUT design can be carried out in four different phases such as geometry phase, meshing phase, solution setup phase and modelling phase which are presented here as follows.

3.1 Phase-I: Geometry Selection

Ansys fluent 15 software pack with full version was used for modelling SUT design with prototype dimensions as shown in table 1. The corresponding geometry can be modelled by opening fluent in Ansys 15 workbench wherein by selecting, geometry → 2D analysis model → XY plane → optional selection of angles and parameters can be further selected for modification. Using this procedure, SUT design based on the opted parametric dimensions displayed in table 1 can be simulated. After attaining the desired tower structure, one can save the same by procedural clicking of options in menu bar → concept → sketches → surface → generate → save the SUT design in a folder.

Table 1. Dimensions of SUT prototype.

Parameters	Dimensions
Height of the tower	2 m
Length of the base	3.2 m
Diameter of the tower	0.4 m
Angle of canopy	0,5,10 degrees
Height of the inlet	0.127,0.15,0.17 m

3.2. Phase-II: Meshing

After completing the geometry, select the mesh option in the Ansys workbench. Meshing is a process that involves dimension setup, refinement, face mapping of the desired structure (SUT) usually achieved by fragmenting the desired component into similar individual panel components to study the uniform distribution effect of applied load on the entire structural composition. Since each element has its own stiffness while loading, the stress developed on the entire structure can be calculated by summing up all individual stiffness's of the components to attain global stiffness matrix.

The mesh of each part in SUT is generated separately as its components can be split into three different zones i.e. canopy zone, transition section between canopy and tower zone. A secondary refinement of the mesh can be considered when panel size is too wide or sensitive to obtain better quality of the mesh. As an example, a strong pressure gradient will exist at the transition zone i.e. between canopy and tower zone where secondary refinement is recommended due to its sensitiveness in the computational domain. Finally, skewness ratio is examined to check desired mesh quality. Here the system geometry considered for examination consists of tower with height 2 meters (m) and 0.4 m diameter having a base length of 3.2 m and provision to vary not only the orientation of canopy angle between 0°-10° but also the height of the inlet between 0.127 m to 0.17 m.

3.3 Phase-III: Solution Setup

Once the geometry and meshing were done for desired SUT structure, general settings for the solution setup has to be applied by opting Ansys workbench 15 → click on Solution setup → launch fluent with double precision. The general setting applied for examination is showed in table 2.

Table 2. Solution setup general settings.

Type	Pressure based
Velocity formulation	Absolute
Type	Steady
2D space	Planar
Gravitational acceleration	-9.8 m/s ²

3.4 Phase-IV: Modeling

After completing the above three phases successfully, the presumptions required for the SUT modeling has to be carried out by choosing requisite options and setting desired options such as Energy equation → ON, K-Epsilon model with standard mode with buoyancy effect [6], select air as material (boussinesq) [7], Operating conditions → 300K, insertion of boundary conditions like insolation (heat flux) values at different parts, setting solution initialization as standard initialization. Finally, clicking on 'Run calculations' by insertion of desired value for number of iterations to be carried out.

4. Results and Discussion

By following the above-mentioned procedure, simulation results can be obtained where contour maps and graphs pertaining to different parameters under consideration can be observed for desired SUT power plant structure. Here it is intended to analyze the variations in basic physical parameters such as temperature, pressure and velocity by varying the canopy angles and insolation levels to explore their interdependence for extracting maximum power output. The following observations were noticed [8] while carrying out parametric study on the original design of the simulation prototype.

4.1 Contour maps at 0° canopy angle and 600 Wm⁻²

Figure 1a, 1b and 1c represents contour maps of variation in pressure, temperature and air velocity at 0° canopy angle and 600 Wm⁻² while table 3 displays variations in pressure, temperature and velocity with respect to variation in height at 0° canopy angle at 600 Wm⁻² insolation. From figure 1a, it can be observed that the pressure is least at center of the tower and increases with increase in the height of the tower. Pressure varies from inlet to the outlet of the tower which creates an updraft and leads to mass flow in the tower wherever pressure difference occurs. From figure 1b, it can be noticed that, as the heat flux emanate from the base, the temperature below the canopy is identified to be more than the outside temperature and the temperature at inlet of the tower is identified to be maximum whereas with the increase in height of the tower, there is a decrease in the value of temperature. From figure 1c, it is clearly evident that air velocity remains constant throughout the tower but there is a change in velocity at middle and bottom of the tower with maximum velocity at a height of 0.3 m, indicating suitability for turbine placement position to attain maximum turbine efficiency.

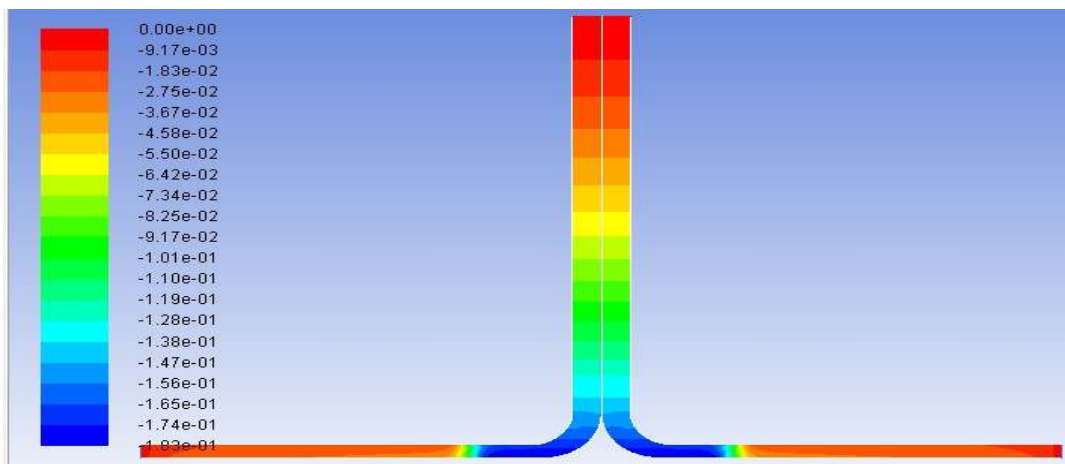


Figure 1a. Pressure contour maps of SUT at 0° canopy angle and 600 Wm⁻².

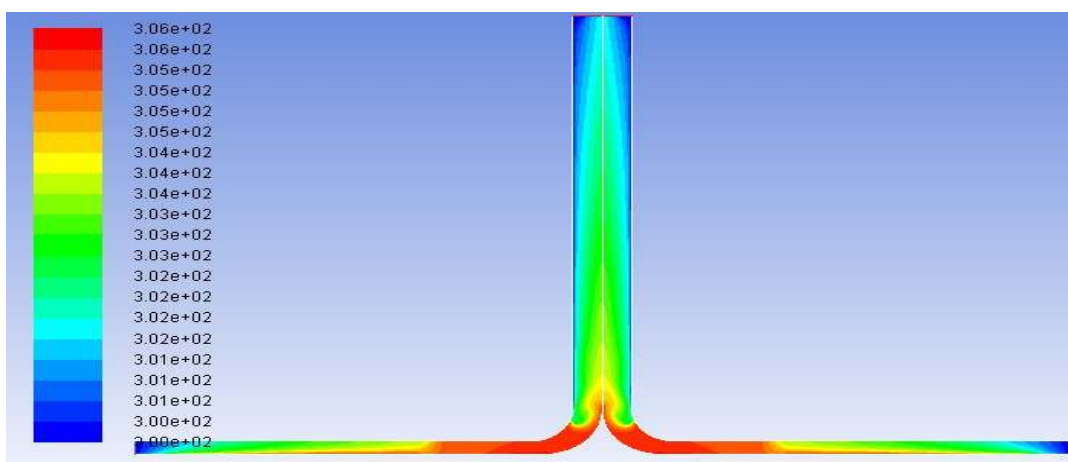


Figure 1b. Temperature contour maps of SUT at 0° canopy angle and 600 Wm⁻².

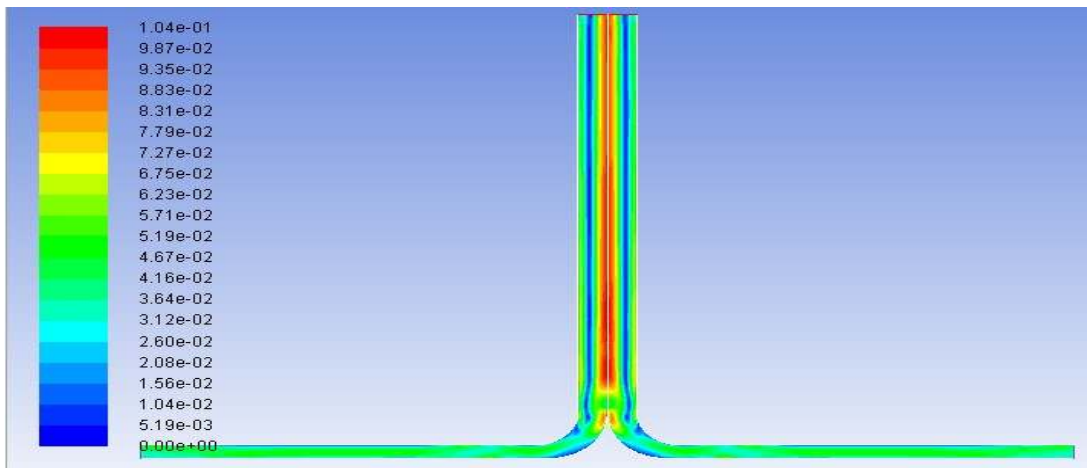


Figure 1c. Air velocity contour maps of SUT 0° canopy angle and 600 Wm⁻².

Table 3. Parametric values for constant insolation at 0° canopy value (without slope).

Height (m)	Pressure (Pa)	Temperature (K)	Velocity (ms ⁻¹)
0.5	-0.08	303.3	0.105
1	-0.045	302.5	0.101
1.5	-0.02	302	0.098
2	0	301.7	0.096

4.2 Pressure contour maps obtained at 5° canopy angle with varying Insolation

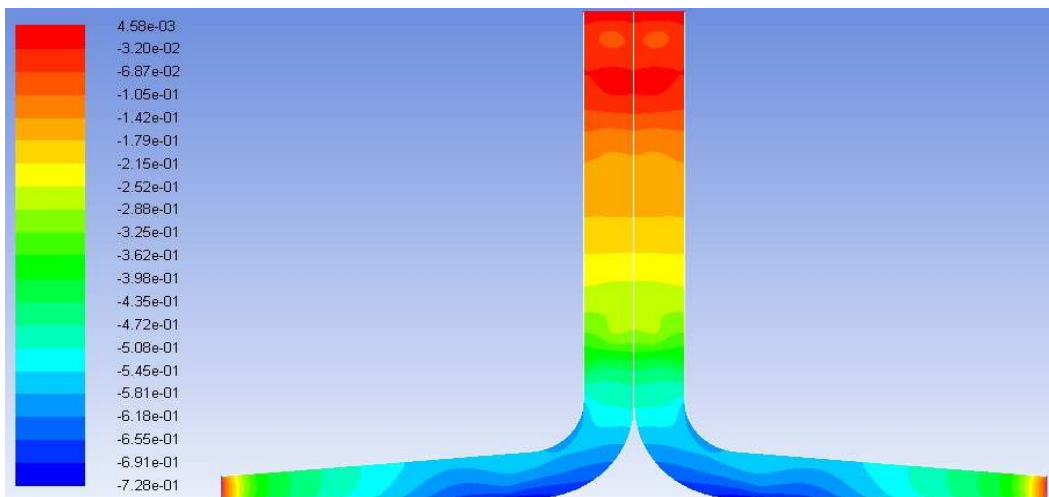


Figure 2a. Pressure contour maps of SUT plant at 600 Wm⁻² at 5° canopy value.

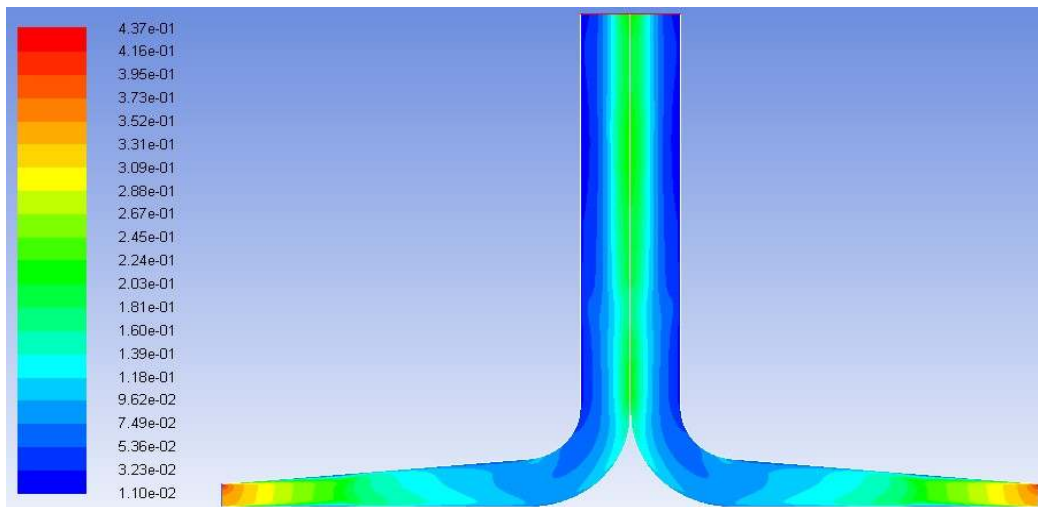


Figure 2b. Pressure contour maps of SUT plant at 800 Wm^{-2} at 5° canopy value.

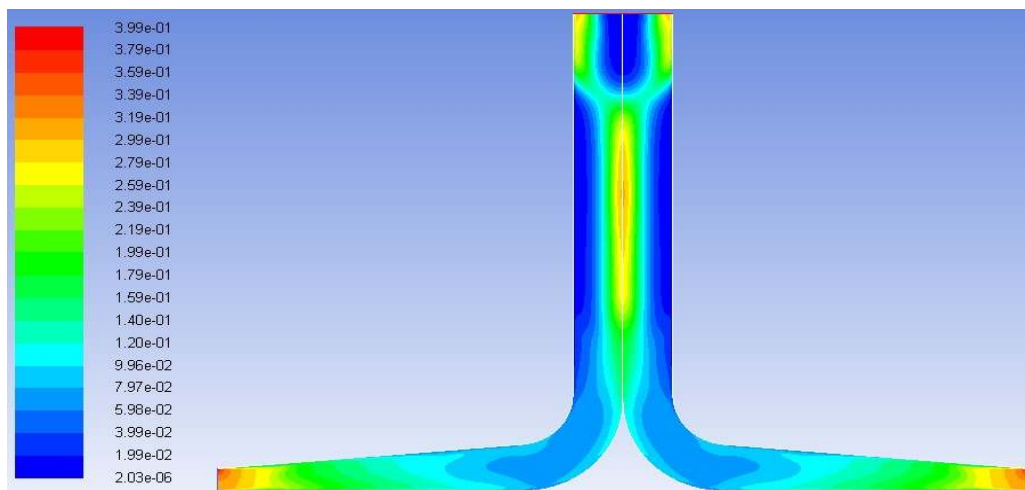


Figure 2c. Pressure contour maps of SUT plant at 1000 Wm^{-2} at 5° canopy value.

Table 4. Pressure values for different insolation at 5° canopy angle.

Height (m)	600 Wm^{-2}	800 Wm^{-2}	1000 Wm^{-2}
0.5	-0.52	-0.26	-0.22
1	-0.28	-0.19	-0.18
1.5	-0.14	-0.13	-0.11
2	-0.06	-0.04	0.2

Figure 2a, 2b and 2c represents contour maps of variation in pressure at 5° canopy angle with respect to varying insolation at 600 Wm^{-2} , 800 Wm^{-2} and 1000 Wm^{-2} while table 4 displays variations in pressure with respect to variation in height of the tower at 5° canopy angle at different insolation levels of

600 Wm^{-2} , 800 Wm^{-2} and 1000 Wm^{-2} . From figure 2a, it can be observed that the pressure at the inlet of the tower is low and gradually increase at the outlet of the tower. Thus, pressure difference is created in the tower. From the figure 2b it can be noticed that at 800 Wm^{-2} , pressure at the inlet of the tower is low and gradually increase at the outlet of the tower there by creating pressure difference in the tower. From figure 2c, it is clearly evident that the pressure at the inlet of the tower is low and gradually increases towards the outlet of the tower. Thus, pressure difference is created in the tower.

4.3. Temperature contours obtained for different insolation values

Figure 3a, 3b and 3c represents contour maps of variation in temperature at 5° canopy angle with respect to varying insolation at 600 Wm^{-2} , 800 Wm^{-2} and 1000 Wm^{-2} while table 5 displays variations in temperature with respect to variation in height of the tower at 5° canopy angle at different insolation levels of 600 Wm^{-2} , 800 Wm^{-2} and 1000 Wm^{-2} . From figure 3a, it can be observed that at 600 Wm^{-2} insolation, change in temperature is low with maximum temperature at the base due to absorption and reflection of solar radiation beneath the canopy. From figure 3b i.e. at 800 Wm^{-2} insolation, no significant change with respect to figure 3a except that tower temperature slightly increases when compared to temperature beneath the canopy. From figure 3c i.e. at 1000 Wm^{-2} , it is clearly evident that temperature inside the tower is more than the canopy temperature.

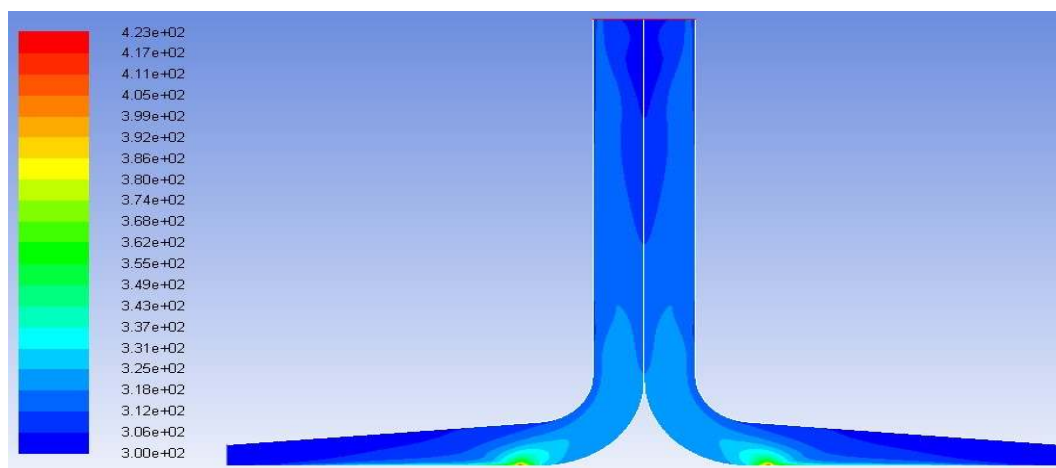


Figure 3a. Temperature contour maps of SUT plant at 600 Wm^{-2} at 5° canopy value angle.

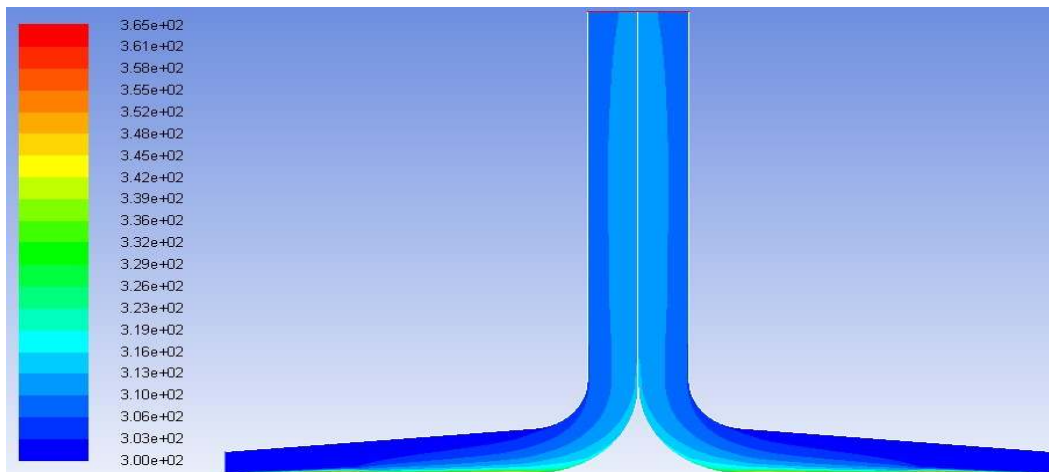


Figure 3b. Temperature contour maps of SUT plant at 800 Wm^{-2} at 5° canopy angle.

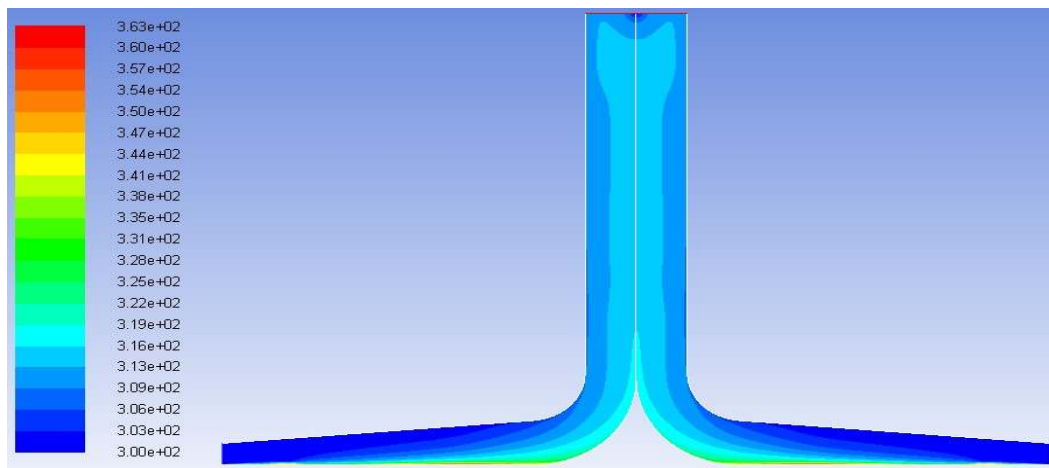


Figure 3c. Temperature contour maps of SUT plant at 1000 Wm^{-2} at 5° canopy angle.

Table 5. Temperature values for different insolation levels at 5° canopy value.

Height (m)	600 Wm^{-2}	800 Wm^{-2}	1000 Wm^{-2}
0.5	309.5	313	315.8
1	307	311.5	314.4
1.5	304	310.5	313.6
2	303.5	310	313.2

4.4. Velocity contours obtained for different insolation values

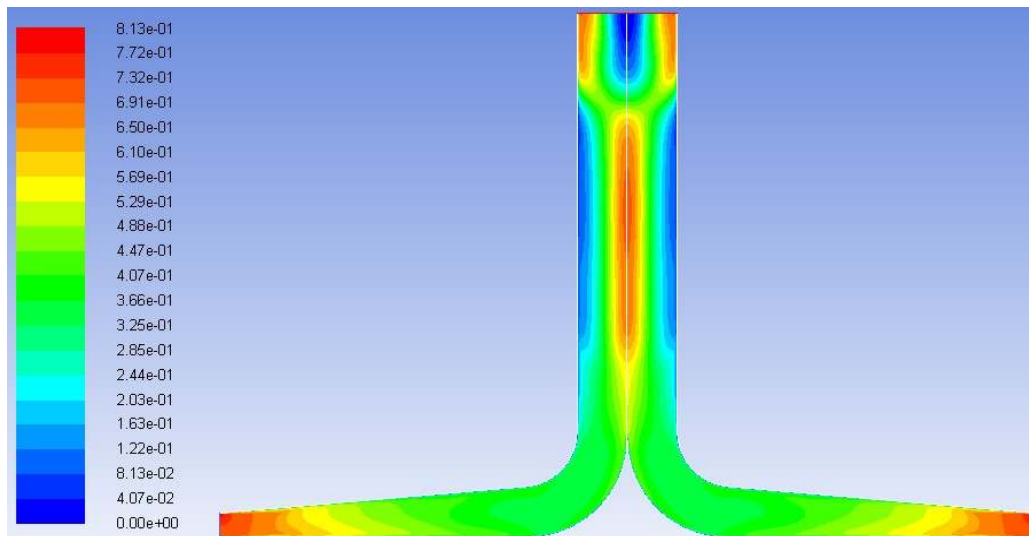


Figure 4a. Velocity contour maps of SUT plant at 600 Wm^{-2} at 5° canopy angle.

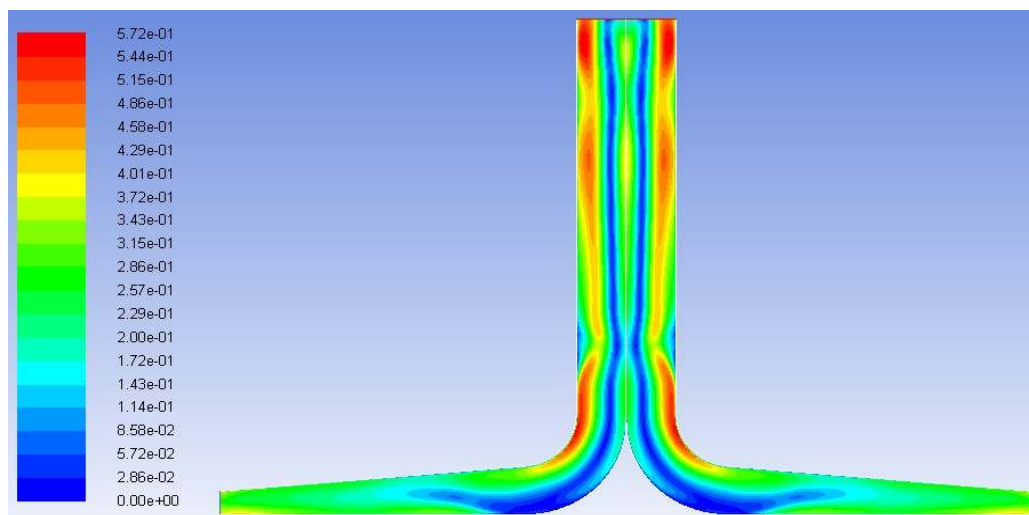


Figure 4b. Velocity contour maps of SUT plant at 800 Wm^{-2} at 5° canopy angle

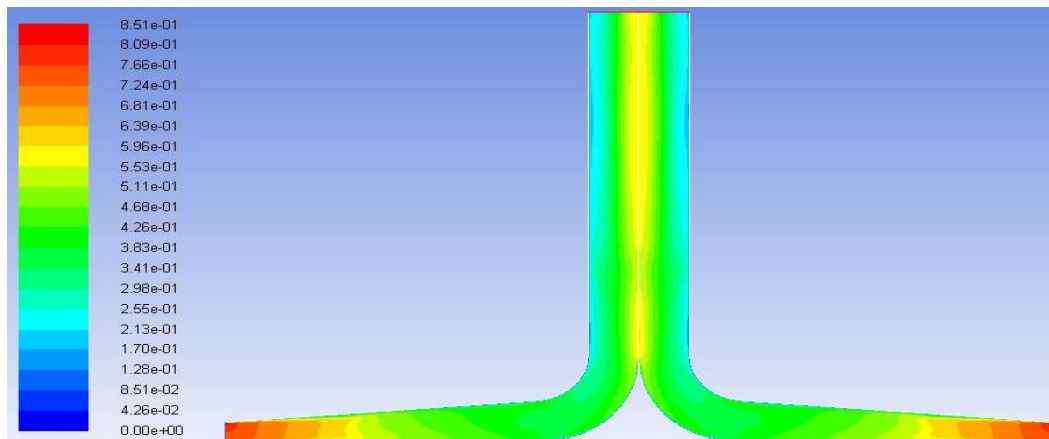


Figure 4c. Velocity contour maps of SUT plant at 1000 Wm^{-2} at 5° canopy angle.

Table 6. Velocity values for different insolation levels at 5° canopy value.

Height (m)	600 Wm^{-2}	800 Wm^{-2}	1000 Wm^{-2}
0.5	0.19	0.5	0.58
1	0.16	0.51	0.62
1.5	0.25	0.56	0.65
2	0.21	0.55	0.68

Figure 4a, 4b and 4c represents contour maps of variation in velocity profile at 5° canopy angle with respect to varying insolation at 600 Wm^{-2} , 800 Wm^{-2} and 1000 Wm^{-2} while table 6 displays variations in velocity with respect to variation in height of the tower at 5° canopy angle at different insolation levels of 600 Wm^{-2} , 800 Wm^{-2} and 1000 Wm^{-2} . From figure 4a, a maximum velocity at the center of the tower can be observed that at 600 Wm^{-2} and 800 Wm^{-2} insolation levels, indicating suitability of turbine placement for attaining maximum efficiency whereas at 1000 Wm^{-2} , maximum velocity at the inlet periphery of the collector can be clearly noticed from figure 4c, indicating desirable placement of turbine to extract maximum efficiency with an option to place more than one turbine.

4.5 Contour maps obtained at 10° canopy angle

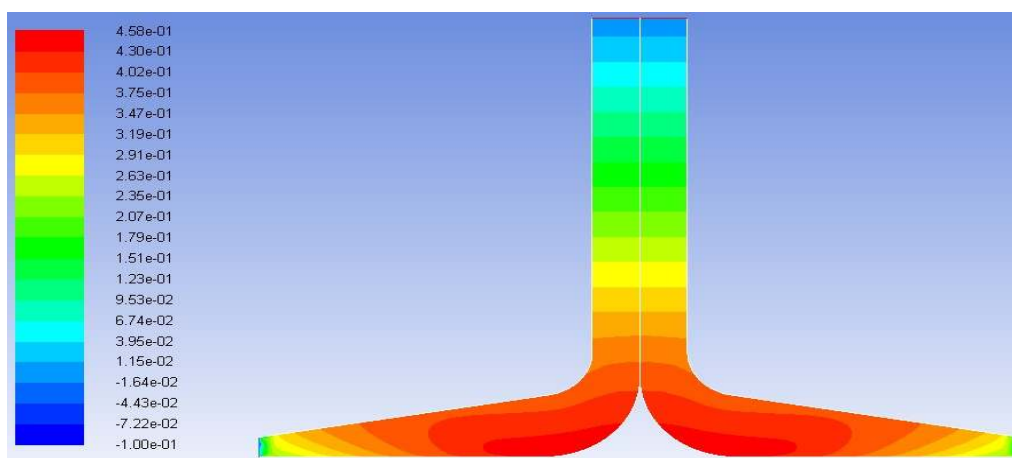


Figure 5a. Pressure contour maps of SUT plant at 600 Wm^{-2} at 10° canopy angle.

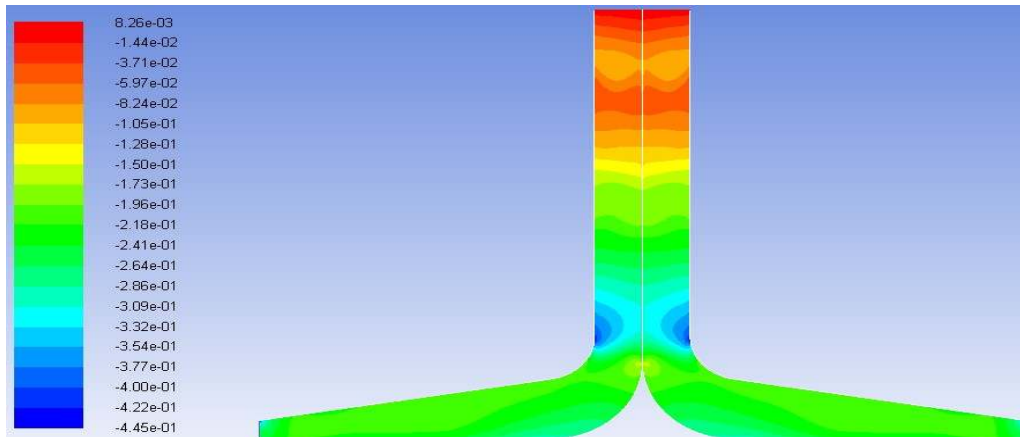


Figure 5b. Pressure contour maps of SUT plant at 800 Wm^{-2} at 10° canopy angle.

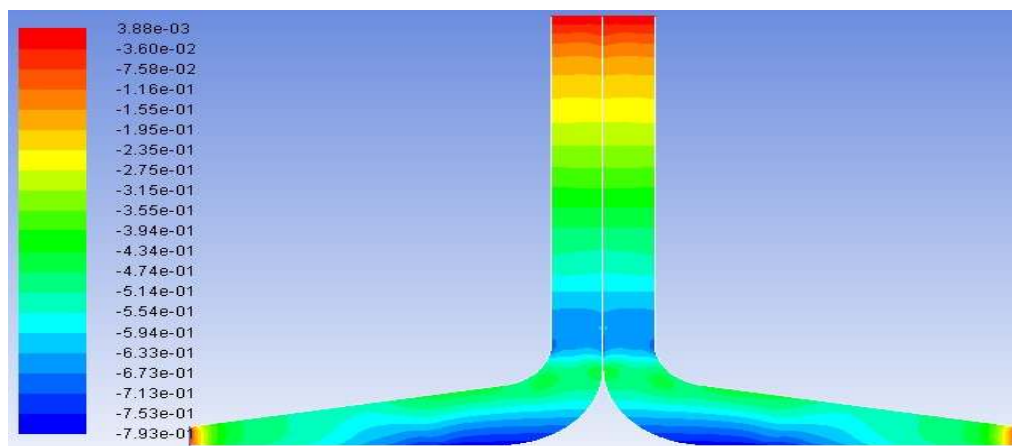


Figure 5c. Pressure contour maps of SUT plant at 1000 Wm^{-2} at 10° canopy angle.

Table 7. Pressure values for different insolation levels at 10° canopy value.

Height (m)	600 Wm^{-2}	800 Wm^{-2}	1000 Wm^{-2}
0.5	-0.41	-0.34	-0.28
1	-0.26	-0.24	-0.21
1.5	-0.15	-0.12	-0.1
2	-0.04	-0.03	0.02

Figure 5a, 5b and 5c represents contour maps of variation in pressure profile at 10° canopy angle with respect to variation in insolation at 600 Wm^{-2} , 800 Wm^{-2} and 1000 Wm^{-2} while table 7 displays variations in pressure with respect to variation in height of the tower at 10° canopy angle at different insolation levels of 600 Wm^{-2} , 800 Wm^{-2} and 1000 Wm^{-2} . At 600 Wm^{-2} , it can be observed that the pressure at inlet of the tower is high and gradually decreases at the outlet of the tower from figure 5a thereby allowing air flow within the tower due to pressure difference. By examining the figure 5b and figure 5c i.e. at 800 Wm^{-2} and 1000 Wm^{-2} insolation levels, pressure at the inlet of the tower is observed to be low and increases gradually at the outlet of the tower leading to occurrence of pressure difference within the tower.

4.6 Temperature contours obtained for different insolation values

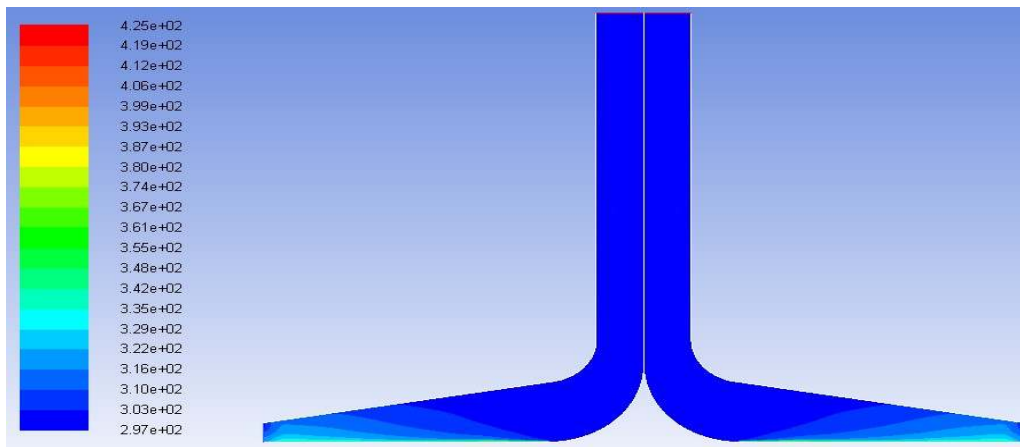


Figure 6a. Temperature Contour maps of SUT plant at 600 Wm^{-2} at 10° canopy angle.

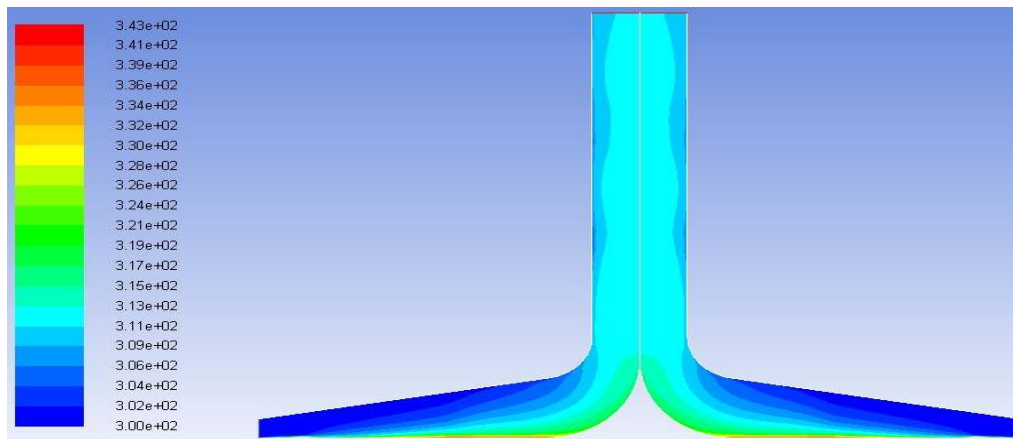


Figure 6b. Temperature Contour maps of SUT plant at 800 Wm^{-2} at 10° canopy angle.

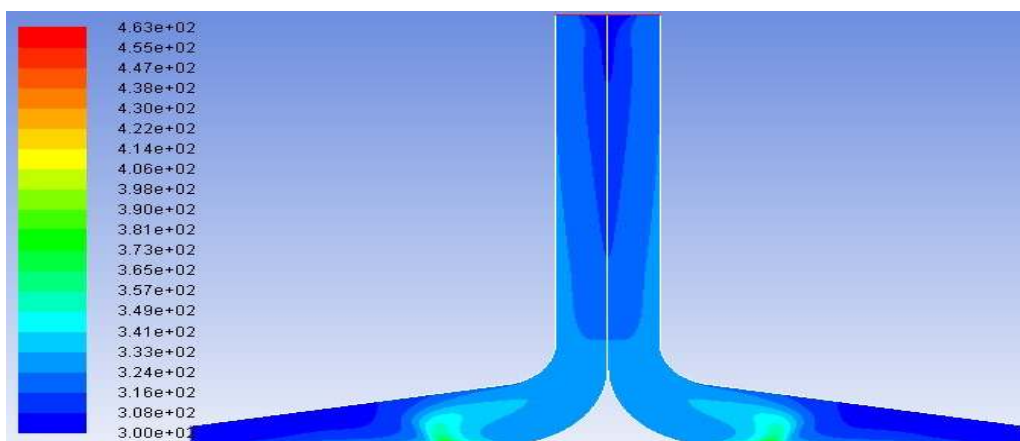


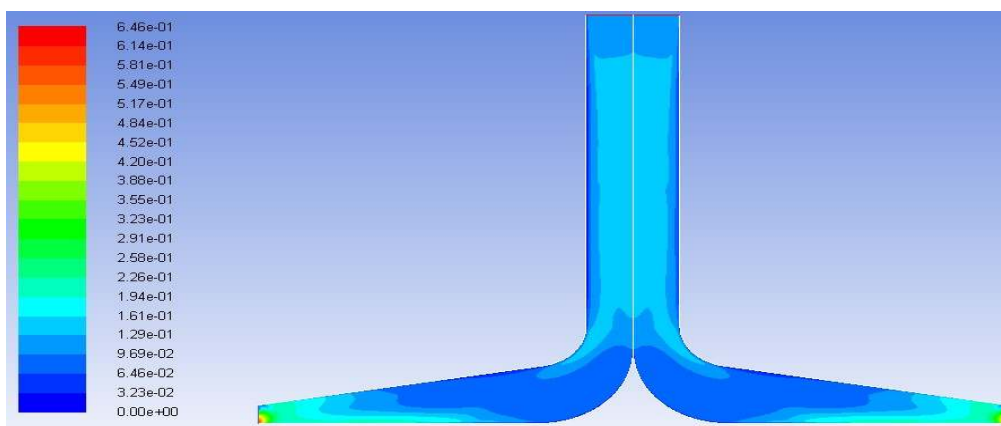
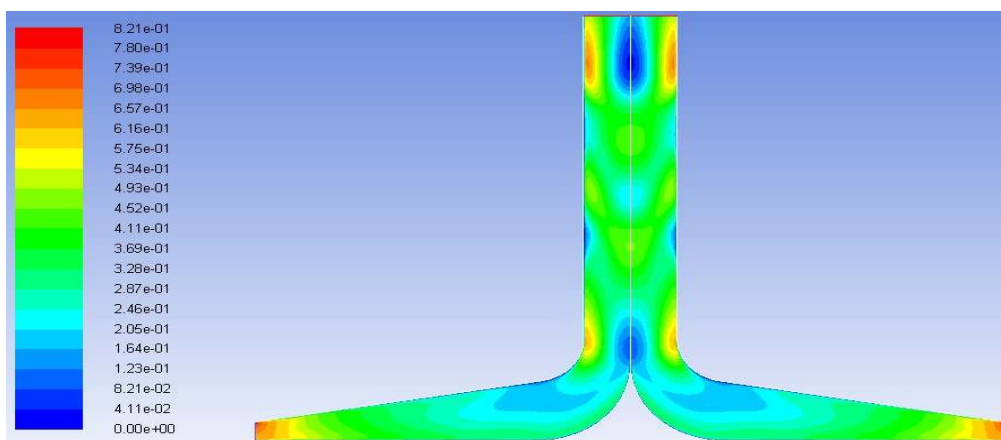
Figure 6c. Temperature Contour maps of SUT plant at 1000 Wm^{-2} at 10° canopy angle.

Table 8. Temperature values for different insolation levels at 10° canopy value.

Height (m)	600 Wm^{-2}	800 Wm^{-2}	1000 Wm^{-2}
0.5	309	317.1	327.5
1	307	311.8	317
1.5	306	311.6	313.3
2	305	311.2	312.1

Figure 6a, 6b and 6c represents contour maps of variation in temperature profile of SUT at 10° canopy angle with respect to variation in insolation at 600 Wm^{-2} , 800 Wm^{-2} and 1000 Wm^{-2} while table 8 displays variations in temperature with respect to variation in height of the tower at 10° canopy angle at different insolation levels of 600 Wm^{-2} , 800 Wm^{-2} and 1000 Wm^{-2} . At 600 Wm^{-2} insolation i.e. from figure 6a, it can be observed that the temperature at the base is high due absorption of incoming radiation and reflection from base beneath the canopy whereas at 800 Wm^{-2} and 1000 Wm^{-2} insolation, no significant change with respect to figure 6a, except that the inside temperature of tower is slightly more than temperature corresponding to area underneath canopy.

4.7 Velocity contours obtained for different insolation values

**Figure 7a.** Velocity contour maps of SUT plant at 600 Wm^{-2} at 10° canopy angle.**Figure 7b.** Velocity contour maps of SUT plant at 800 Wm^{-2} at 10° canopy angle.

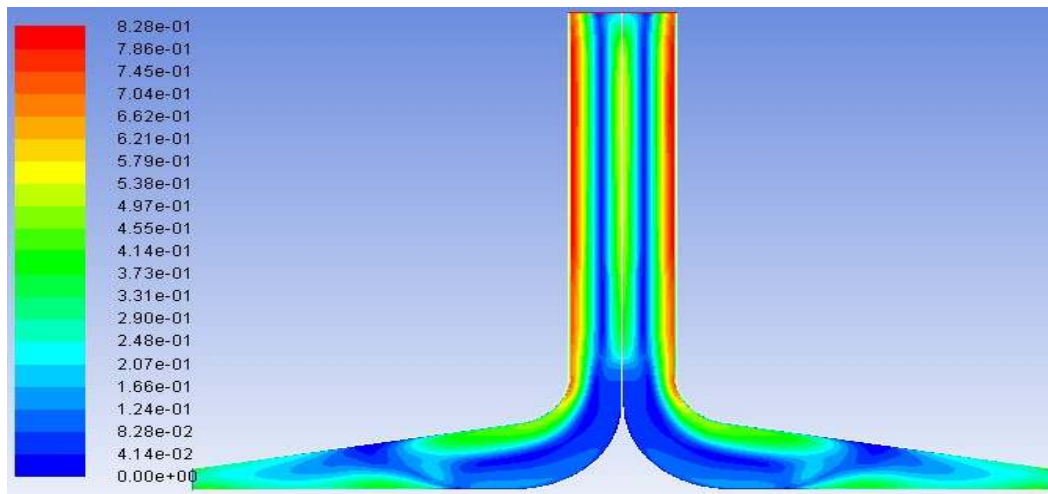


Figure 7c. Velocity contour maps of SUT plant at 1000 Wm^{-2} at 10° canopy angle.

Table 9. Velocity values for different insolation levels at 10° canopy value.

Height (m)	600 Wm^{-2}	800 Wm^{-2}	1000 Wm^{-2}
0.5	0.102	0.12	0.14
1	0.140	0.26	0.34
1.5	0.136	0.28	0.38
2	0.130	0.08	0.36

Figure 7a, 7b and 7c represents contour maps of variation in velocity profile (blue color in the legend) of SUT at 10° canopy angle with respect to variation in insolation at 600 Wm^{-2} , 800 Wm^{-2} and 1000 Wm^{-2} while table 9 displays variations in velocity with respect to variation in height of the tower at 10° canopy angle at different insolation levels of 600 Wm^{-2} , 800 Wm^{-2} and 1000 Wm^{-2} .

At 600 Wm^{-2} insolation level i.e. from figure 7a maximum velocity at the center of the tower can be observed, indicating the suitability of turbine placement for maximum efficiency. From figure 7b, at 800 Wm^{-2} maximum velocity inside the tower can be examined in addition to distribution of velocity profile across the tower due to enhanced recirculation of air inside the tower. Although velocity remains constant, velocity maximum can be noticed at the inlet of the collector thereby indicating suitability of turbine placement beneath the canopy for attaining maximum efficiency of SUT while a constant velocity profile with a maximum velocity at the inlet of the collector. Here it should be noticed that power generated by the turbine may decrease due to recirculation of air.

5. Conclusion

Simulation was conducted using the Ansys fluent software, which solved the energy equation using the Boussinesq approximation. The standard k - ϵ turbulence model was used together incorporating the solar ray tracing model for a more accurate result.

The inlet and outlet ambient temperature was assumed at 300 K. All walls were considered as adiabatic except for the solar collector and the soil cover beneath the solar collector. The solar collector modeling parameters were defined as non-slip, convective heat transfer and radiation. And as for the soil layer, it was assumed as a thermal storage with a heat absorption coefficient of 0.8. The numerical model was also validated using previous numerical results obtained from IIT Dhanbad and Marian College of engineering Thiruvananthapuram.

The parametric study was conducted for the angle of inclination of the slope collector, with fixed height of the solar tower configuration with either a fixed entrance or a fixed exit and different solar radiation for the optimized geometry. The objective of varying these angles and insolation is to determine the most suitable position for installation of the power generation turbine. It was important to have a high velocity at the upstream of the turbine. The power generation turbine utilized the updraft velocity, which means the greater the velocity, the faster the turbine can turn to generate more power.

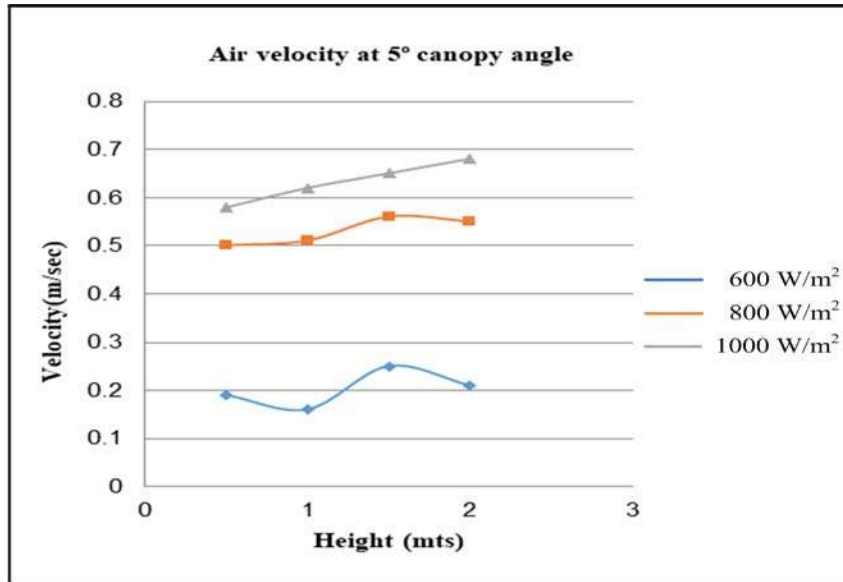


Figure 8a. Air velocity vs Height at 5° canopy angle.

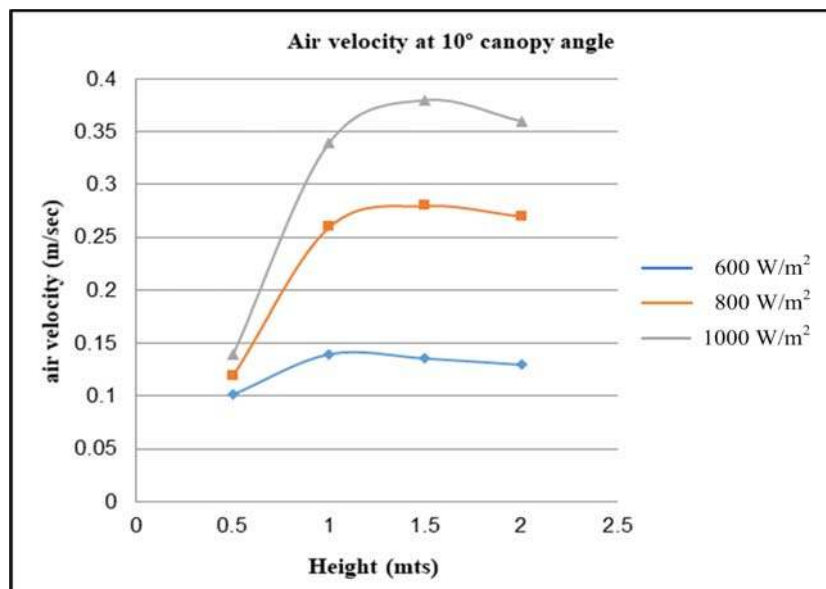


Figure 8b. Air velocity vs Height at 10° canopy angle.

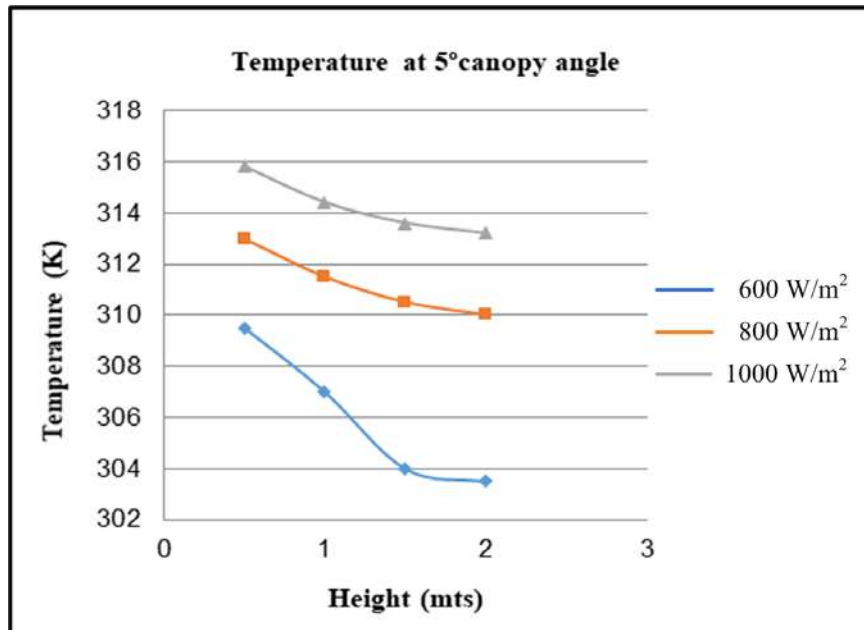


Figure 9a. Temperature vs Height at 5° canopy angle.

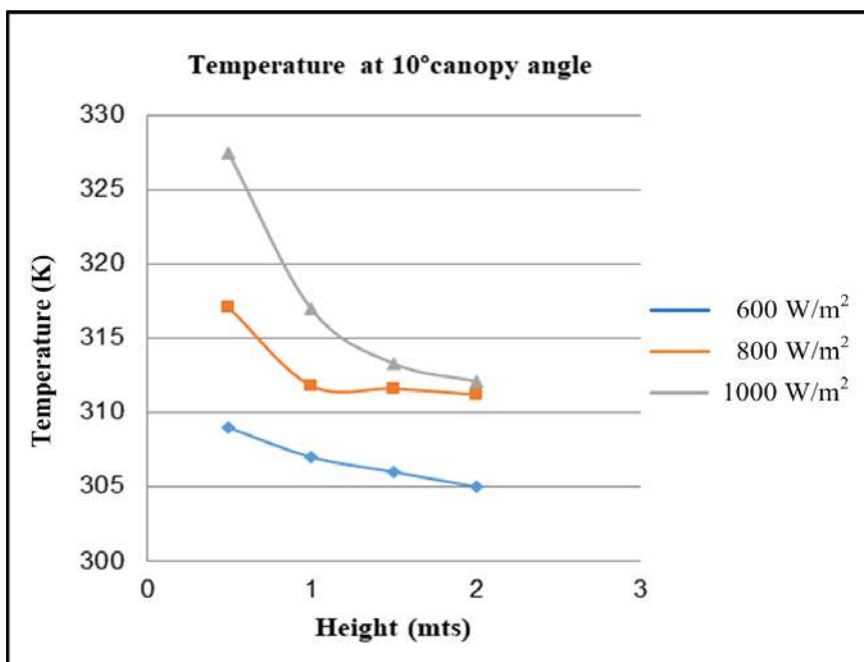


Figure 9b. Temperature vs Height at 10° canopy angle.

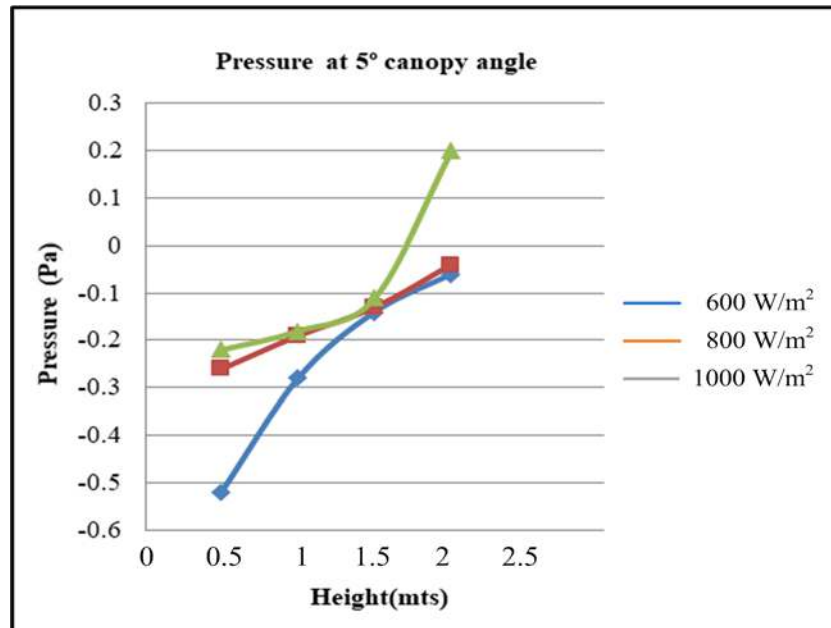


Figure 10a. Pressure vs Height at 5° canopy angle.

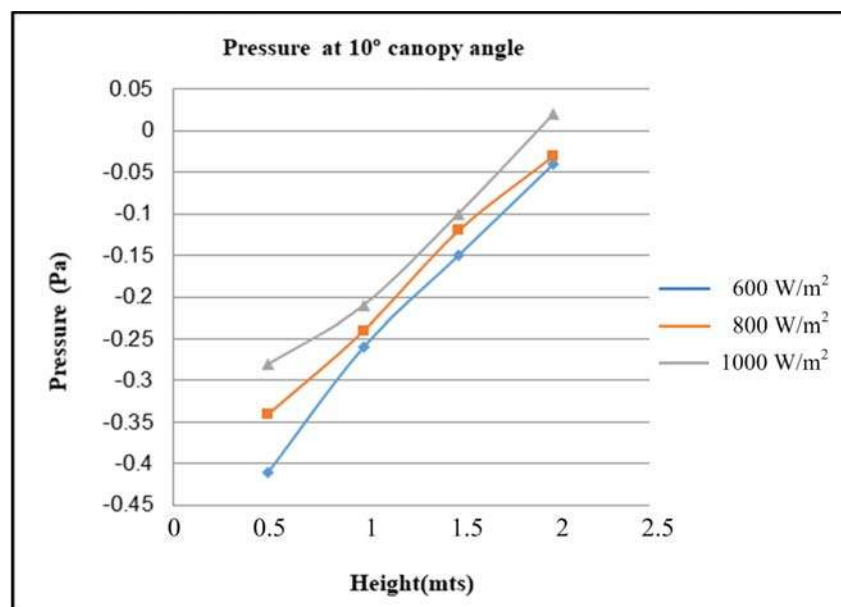


Figure 10b. Pressure vs Height at 10° canopy angle.

Figures 8a, 9a and 10a represents the parametric relationships of air velocity, temperature and pressure with respect to variation in height at 5° canopy angle while figures 8b, 9b and 10b represents the parametric relationships of air velocity, temperature and pressure with respect to variation in height at 10° canopy angle. From these figures, one can clearly notice that, it is possible to determine the most suitable position for installation of the power generation turbine by deploying site specific design consideration values in Ansys fluent software to extract maximum efficiency from SUT. This simulation was carried out to analyze the performance of the SUT using a two-dimensional steady state and energy equation. The air flow inside the updraft tower was assumed as to be planar where it was simulated with k-epsilon model

using Ansys Fluent software. The above results are validated and selection of canopy angle depending on the latitude and longitude of a specific location can yield desired results in successful implementation of SUT power plant.

Acknowledgments: The authors express their gratitude to the JNT University, Kakinada, and Smart Grid Research Lab, Vellore Institute of Technology, Vellore, India for their entire support towards this research work.

References

- [1]. Sitharthan R, Geethanjali M and Pandey TKS 2016 Adaptive protection scheme for smart microgrid with electronically coupled distributed generations *Alexandria Engineering Journal* **55(3)** 2539-2550
- [2]. Fathima AH, and Palanisamy K 2014 Battery energy storage applications in wind integrated systems—a review *IEEE International Conference on Smart Electric Grid* 1-8
- [3]. Prabakaran N and Palanisamy K 2015 Investigation of single-phase reduced switch count asymmetric multilevel inverter using advanced pulse width modulation technique *International Journal of Renewable Energy Research* **5(3)** 879-890.
- [4]. Jerin ARA, Kaliannan P and Subramaniam U 2017 Improved fault ride through capability of DFIG based wind turbines using synchronous reference frame control based dynamic voltage restorer. *ISA transactions* **70** 465-474
- [5]. Sitharthan, R, Sundarabalan CK, Devabalaji KR, Nataraj SK and Karthikeyan M 2018 Improved fault ride through capability of DFIG-wind turbines using customized dynamic voltage restorer *Sustainable cities and society* **39** 114-125
- [6]. Prabakaran N and Palanisamy K 2016 A single-phase grid connected hybrid multilevel inverter for interfacing photo-voltaic system *Energy Procedia* **103** 250-255
- [7]. Palanisamy K, Mishra JS, Raglend IJ and Kothari DP 2010 Instantaneous power theory based unified power quality conditioner (UPQC) *IEEE Joint International Conference on Power Electronics, Drives and Energy Systems* 1-5
- [8]. Sitharthan R and Geethanjali M 2017 An adaptive Elman neural network with C-PSO learning algorithm-based pitch angle controller for DFIG based WECS *Journal of Vibration and Control* **23(5)** 716-730
- [9]. Sitharthan R and Geethanjali M 2015 Application of the superconducting fault current limiter strategy to improve the fault ride-through capability of a doubly-fed induction generator-based wind energy conversion system *Simulation* **91(12)** 1081-1087
- [10]. Sitharthan R, Karthikeyan M, Sundar DS and Rajasekaran S 2020 Adaptive hybrid intelligent MPPT controller to approximate effectual wind speed and optimal rotor speed of variable speed wind turbine *ISA transactions* **96** 479-489
- [11]. Sitharthan R, Devabalaji KR and Jeon A 2017 An Levenberg–Marquardt trained feed-forward back-propagation based intelligent pitch angle controller for wind generation system *Renewable Energy Focus* **22** 24-32
- [12]. Sitharthan R, Sundarabalan CK, Devabalaji KR, Yuvaraj T and Mohamed Imran A 2019 Automated power management strategy for wind power generation system using pitch angle controller *Measurement and Control* **52(3-4)** 169-182
- [13]. Sundar DS, Umamaheswari C, Sridarshini T, Karthikeyan M, Sitharthan R, Raja AS and Carrasco MF 2019 Compact four-port circulator based on 2D photonic crystals with a 90° rotation of the light wave for photonic integrated circuits applications *Laser Physics* **29(6)** 066201

- [14]. Sitharthan R, Parthasarathy T, Sheeba Rani S and Ramya KC 2019. An improved radial basis function neural network control strategy-based maximum power point tracking controller for wind power generation system *Transactions of the Institute of Measurement and Control* **41(11)** 3158-3170
- [15]. Rajesh M and Gnanasekar JM 2017 Path observation based physical routing protocol for wireless ad hoc networks *Wireless Personal Communications* **97(1)** 1267-1289
- [16]. Palanisamy K, Varghese LJ, Raglend IJ and Kothari DP 2009. Comparison of intelligent techniques to solve economic load dispatch problem with line flow constraints *IEEE International Advance Computing Conference* 446-452
- [17]. Sitharthan R, Ponnusamy M, Karthikeyan M and Sundar DS 2019 Analysis on smart material suitable for autogenous microelectronic application *Materials Research Express* **6(10)** 105709
- [18]. Rajaram R, Palanisamy K, Ramasamy S and Ramanathan P 2014 Selective harmonic elimination in PWM inverter using fire fly and fireworks algorithm *International Journal of Innovative Research in Advanced Engineering* **1(8)** 55-62
- [19]. Sitharthan R, Swaminathan JN and Parthasarathy T 2018 March. Exploration of wind energy in India: A short review *IEEE National Power Engineering Conference* 1-5
- [20]. Karthikeyan M, Sitharthan R, Ali T and Roy B 2020 Compact multiband CPW fed monopole antenna with square ring and T-shaped strips *Microwave and Optical Technology Letters* **62(2)** 926-932
- [21]. Sundar D Sridarshini T, Sitharthan R, Madurakavi Karthikeyan, Sivanantha Raja A, and Marcos Flores Carrasco 2019 Performance investigation of 16/32-channel DWDM PON and long-reach PON systems using an ASE noise source *In Advances in Optoelectronic Technology and Industry Development: Proceedings of the 12th International Symposium on Photonics and Optoelectronics* 93
- [22]. Sitharthan R and Geethanjali M 2014 Wind Energy Utilization in India: A Review *Middle-East J. Sci. Res.* **22** 796–801 doi:10.5829/idosi.mejsr.2014.22.06.21944
- [23]. Sitharthan R and Geethanjali M 2014 ANFIS based wind speed sensor-less MPPT controller for variable speed wind energy conversion systems *Australian Journal of Basic and Applied Sciences* **8**14-23
- [24]. Jerin ARA, Kaliannan P, Subramaniam U and El Moursi MS 2018 Review on FRT solutions for improving transient stability in DFIG-WTs *IET Renewable Power Generation* **12(15)** 1786-1799
- [25]. Prabakaran N, Jerin ARA, Palanisamy K and Umashankar S 2017 Integration of single-phase reduced switch multilevel inverter topology for grid connected photovoltaic system *Energy Procedia* **138** 1177-1183
- [26]. Rameshkumar K, Indragandhi V, Palanisamy K and Arunkumari T 2017 Model predictive current control of single phase shunt active power filter *Energy Procedia* **117** 658-665
- [27]. Fathima AH and Palanisamy K 2016 Energy storage systems for energy management of renewables in distributed generation systems *Energy Management of Distributed Generation Systems* 157
- [28]. Rajesh M 2020 Streamlining Radio Network Organizing Enlargement Towards Microcellular Frameworks *Wireless Personal Communications* 1-13
- [29]. Subbiah B, Obaidat MS, Sriram S, Manoharn R and Chandrasekaran SK 2020 Selection of intermediate routes for secure data communication systems using graph theory application and grey wolf optimisation algorithm in MANETs *IET Networks* doi:10.1049/iet-net.2020.0051
- [30]. Singh RR and Chelliah TR 2017 Enforcement of cost-effective energy conservation on single-fed asynchronous machine using a novel switching strategy *Energy* **126** 179-191

- [31]. Amalorpavaraj RAJ, Palanisamy K, Umashankar S and Thirumoorthy AD 2016 Power quality improvement of grid connected wind farms through voltage restoration using dynamic voltage restorer *International Journal of Renewable Energy Research* **6(1)** 53-60
- [32]. Singh RR, Chelliah TR, Khare D and Ramesh US 2016 November. Energy saving strategy on electric propulsion system integrated with doubly fed asynchronous motors *IEEE Power India International Conference* 1-6
- [33]. Sujatha K and Punithavathani DS 2018 Optimized ensemble decision-based multi-focus imagefusion using binary genetic Grey-Wolf optimizer in camera sensor networks *Multimedia Tools and Applications* **77(2)** 1735-1759
- [34]. Krishnamoorthy S, Punithavathani S and Priya JK 2017 Extraction of well-exposed pixels for image fusion with a sub-banding technique for high dynamic range images *International Journal of Image and Data Fusion* **8(1)** 54-72
- [35]. Singh RR, Mohan H and Chelliah TR 2016 November. Performance of doubly fed machines influenced to electrical perturbation in pumped storage plant-a comparative electromechanical analysis *IEEE 7th India International Conference on Power Electronics* 1-6